# Shedding of the endothelial glycocalyx in arterioles, capillaries, and venules and its effect on capillary hemodynamics during inflammation

**Herbert H. Lipowsky, Lujia Gao and Ann Lescanic**

*Am J Physiol Heart Circ Physiol* 301:H2235-H2245, 2011. First published 16 September 2011; doi:10.1152/ajpheart.00803.2011

*Am J Physiol Heart Circ Physiol* 301: H2235–H2245, 2011.
First published September 16, 2011; doi:10.1152/ajpheart.00803.2011.

# Shedding of the endothelial glycocalyx in arterioles, capillaries, and venules and its effect on capillary hemodynamics during inflammation

**Herbert H. Lipowsky, Lujia Gao, and Ann Lescanic**

*Department of Bioengineering, The Pennsylvania State University, University Park, Pennsylvania*

Submitted 10 August 2011; accepted in final form 13 September 2011

**Lipowsky HH, Gao L, Lescanic A.** Shedding of the endothelial glycocalyx in arterioles, capillaries, and venules and its effect on capillary hemodynamics during inflammation. *Am J Physiol Heart Circ Physiol* 301: H2235–H2245, 2011. First published September 16, 2011; doi:10.1152/ajpheart.00803.2011.—The endothelial glycocalyx has been identified as a barrier to transvascular exchange of fluid, macromolecules, and leukocyte-endothelium [endothelial cell (EC)] adhesion during the inflammatory process. Shedding of glycans and structural changes of the glycocalyx have been shown to occur in response to several agonists. To elucidate the effects of glycan shedding on microvascular hemodynamics and capillary resistance to flow, glycan shedding in microvessels in mesentery (rat) was induced by superfusion with $10^{-7}$ M fMLP. Shedding was quantified by reductions of fluorescently labeled lectin (BS-1) bound to the EC and reductions in thickness of the barrier to infiltration of 70-kDa dextran on the EC surface. Red cell velocities (two-slit technique), pressure drops (dual servo-null method), and capillary hematocrit (direct cell counting) were measured in parallel experiments. The results indicate that fMLP caused shedding of glycans in all microvessels with reductions in thickness of the barrier to 70-kDa dextran of 110, 80, and 123 nm, in arterioles, capillaries, and venules, respectively. Intravascular volumetric flows fell proportionately in all three divisions in response to rapid obstruction of venules by white blood cell (WBC)-EC adhesion, and capillary resistance to flow rose 18% due to diminished deformability of activated WBCs. Capillary resistance fell significantly 26% over a 30-min period, as glycans were shed from the EC surface to increase effective capillary diameter, whereas capillary hematocrit and anatomic diameter remained invariant. This decrease in capillary resistance mitigates the increase in resistance due to diminished WBC deformability, and hence these concurrent rheological events may be of equal importance in affecting capillary flow during the inflammatory process.

glycosaminoglycans; glycocalyx thickness; lectin binding; f-Met-Leu-Phe; resistance to flow

THE COATING OF PROTEINS AND polysaccharides on the vascular endothelium has received considerable interest in light of its role as a barrier to transvascular exchange and blood-endothelial interactions. Adsorbed proteins on the endothelial cell (EC) luminal surface, first postulated in studies of capillary permeability by Danielli (12), and a layer of polysaccharides bound to transmembrane and membrane-linked proteins (the glycocalyx), first noted with electron microscopy by Luft (40), serve a multifaceted role in vascular homeostasis (48, 52). This endothelial surface layer is an important barrier to transvascular exchange of water and solutes (1, 24) and sieving of plasma-borne macromolecules (29, 58, 60). The endothelial surface layer also provides binding sites for antithrombin III, tissue factor pathway inhibitors, lipoprotein lipase, vascular endothelial growth factor, fibroblast growth factor, and extracellular superoxide dismutase (52), serves as a barrier to leukocyte-endothelium adhesion (11, 42–44), and acts as a shear stress sensor and regulator of mechanotransduction (17). Experimental manipulations of the structure of the glycocalyx by perfusion of the microvasculature with heparinase have revealed decreases in intravascular resistance to flow (50). Increases in capillary hematocrit ($H_{CAP}$) have been attributed to removal of the glycocalyx in response to perfusion with heparinase (13) and hyaluronidase (7) and the presence of reactive oxygen species derived from oxidized low-density lipoprotein (LDL) (10). Thus the structure of the glycocalyx is a prime determinant of numerous physiological and hemodynamic processes, and maintenance of its stability may preclude the onset of many pathological disturbances (5).

Studies by electron microscopy have suggested that the glycocalyx is a porous layer composed of a matrix of molecules arranged in a regular pattern (55). The most prominent components of the glycocalyx are the glycosaminoglycans (GAGs): heparan sulfate (HS), chondroitin sulfate (CS), and hyaluronan. The principal proteins on the EC surface that bind HS and CS to form the proteoglycans are the transmembrane syndecans and the membrane-bound glypicans (48). The most prevalent proteoglycan, syndecan-1, is one of four members of this family of proteoglycans and is an integral membrane protein composed of an intracellular domain, a transmembrane domain, and an extracellular core (53). Under normal physiological conditions, the structure of the glycocalyx layer is stable, with a molecular composition that represents a dynamic balance between biosynthesis of new glycans and shear-dependent removal of existing constituents. Fluid shear stresses acting on the EC surface may affect the structure of the glycocalyx by either disrupting its molecular constituents, or activation of proteases and lyases synthesized by the endothelium (4, 43).

Shedding of proteoglycans and GAGs from cultured ECs, or their analogs, has been studied in response to a broad spectrum of agonists (9, 16, 18, 31, 45–47). Shedding of HS proteoglycans (namely the ectodomain of syndecans 1–4) has been shown to occur in response to endotoxin (9), serine and/or cystein proteinases (30), complement activation (46), thrombin and growth factors (56), and activation of protein tyrosine kinase by phorbol esters (16). Using hydroxamic acid inhibitors of matrix metalloproteinases, it has been shown that proteolytic cleavage of the syndecan ectodomain results from the concurrent action of multiple intracellular pathways that activate cell surface metalloproteinases (16).

In vivo, the endothelial glycocalyx has been shown to be shed in response to inflammation (25, 43), hyperglycemia (64), endotoxemia and septic shock (26), presence of oxidized LDL (10), TNF-α (8), atrial natriuretic peptide (6), abnormal blood

Address for reprint requests and other correspondence: H. H. Lipowsky, Dept. of Bioengineering, Penn State Univ., 205 Hallowell Bldg., Univ. Park, PA 16802 (e-mail: hhlbio@engr.psu.edu).

shear stress (20, 21), ischemia-reperfusion injury (43), and during bypass surgery (51, 57). These observations have lead to the hypothesis of an underlying connection between integrity of the glycocalyx and vascular homeostasis (43, 64). Shedding of the glycocalyx in response to cytokines and chemoattractants has been shown to occur in all three principal divisions of the microvasculature. It has been shown in arterioles, in response to TNF-α (25); capillaries, in response to TNF-α (25) and oxidized LDL (10); and venules, in response to TNF-α (25) and fMLP (43). These studies were performed in multiple microvascular networks and species: cremaster muscle (10, 25, 43) and skin flap (7) of the hamster, or mesentery of the rat (43). There has also been limited quantization of basic hemodynamic effects of the specific agonist during the shedding process and consistent measurements of structural alterations of the glycocalyx, as, for example, in terms of its thickness. Thus the present studies were undertaken to systematically quantitate agonist-induced shedding of glycans in arteriolar, capillary, and venular divisions of the mesentery of the rat. Parallel studies were performed to evaluate changes in hemodynamic parameters [red cell velocity ($V_{RBC}$)], in the three network divisions, and alterations in the resistance to flow in capillaries, derived from measurement of pressure drops (ΔP) across the capillary network and changes in $H_{CAP}$.

To this end, four separate protocols were employed to study the glycocalyx and hemodynamics in the mesentery (rat), before and following superfusion with fMLP: *1*) fMLP-induced shedding of glycans from arterioles, capillaries, and venules was characterized by staining the microvessel endothelium with a fluorescently labeled lectin to quantify reductions in bound lectin; *2*) thickness of the glycocalyx and network hemodynamics was evaluated from measurements of the exclusion of 70-kDa fluorescent dextran (Dx70) and $V_{RBC}$, respectively; *3*) $H_{CAP}$ were measured by direct cell counting; and *4*) pressure gradients and red cell velocities were simultaneously measured in the true capillaries to compute changes in the resistance to flow. Taken together, these data provide a unified view of the shedding of the glycocalyx and hemodynamics during a well-defined model of the inflammatory process.

## MATERIALS AND METHODS

*Animal preparation.* All animal studies conformed to the Guiding Principles in the Care and Use of Animals established by the American Physiological Society, and all protocols have been approved by the Institutional Animal Care and Use Committee of The Pennsylvania State University.

Male Wistar rats, weighing 250–400 g, were anesthetized with Inactin (120 mg/kg ip), tracheostomized, and allowed to breathe under spontaneous respiration. The right jugular vein and its paired carotid artery were cannulated with polyethylene tubing (PE-50). Supplemental anesthetic was administered via the jugular catheter, as needed, to maintain a surgical plane of anesthesia. The carotid catheter was connected to a strain-gauge pressure transducer to monitor central arterial pressure, which averaged a nominal 125 mmHg. Core temperature was monitored by a rectal probe and was maintained between 36 and 37°C with the aid of a heating pad.

*Intravital microscopy.* The intestinal mesentery was exteriorized through a midline abdominal incision and placed on a glass pedestal to permit viewing under bright-field microscopy by either trans- or incident illumination. The tissue was superfused with HEPES-buffered Ringer solution (pH = 7.4) at a temperature of 37.0°C, with or without the chemoattractant fMLP at a concentration of $10^{-7}$ M. Fluorescence microscopy was performed under incident laser illumination at a wavelength of 488 nm with a dichroic mirror and filters appropriate for fluorescein excitation and emission spectra. Intensity of the laser illumination was controlled with an acousto-optical tunable filter to modulate its intensity and turn it on and off. To minimize photobleaching of the fluorophore, the tissue was excited during digitization of the video scenes for 0.5-s periods. Visual recordings of the mesentery were made with a Yokogawa CSU-10, spinning disk confocal microscope (Solamere Technology, Salt Lake City, UT) using an XR/MEGA-10 intensified charge-coupled device camera (Stanford Photonics, Palo Alto, CA). Output of the camera was digitized and saved to computer disk in tagged image format, with each image being 1,024 × 1,024 pixels in area with a depth in intensity of 10 bits (1,024). Bright-field images were made with tungsten illumination under transmitted light. Fluorescence microscopy images were acquired using a Zeiss ×20/0.50 numerical aperture (NA) water immersion objective, and spanned 170 × 170 μm in the focal plane. For measurements of microvascular hemodynamics, the microscope configuration was changed to view the tissue with a long working distance Leitz UM20/0.33 NA metallurgical objective, with an effective magnification/NA of ×13/0.22 NA (without the use of the glass hemispheres). An analog silicon target video camera was used to guide placement of the velocimeter photodetector and record microvessel diameter.

*Measurement of endothelial surface glycan concentration and glycocalyx thickness.* To obtain an index of the glycan concentration on the EC surface, the lectin *Bandeira Simplicifolia* (BS-1, Sigma, St. Louis, MO) was labeled with Alexa Fluor 488 (Invitrogen, Carlsbad, CA) and infused intravenously via the jugular indwelling catheter. The concentration of labeled lectin averaged 1.56 ± 0.17 (SD) mg/ml in PBS with a molar ratio of fluorophore to protein equal to 17.5 ± 3.9 (SD) mg/ml, for 10 samples. A single bolus of labeled BS-1 was administered intravenously at a dose of 1 ml/kg and allowed to equilibrate for 20 min before intensity measurements on the EC surface were made.

To quantify the thickness of the EC glycocalyx, the method of Henry and Duling (24) was implemented as described previously (19). In brief, a bolus of 0.1% (in 0.15-ml PBS) of fluorescein isothiocyanate labeled Dx70 (Sigma) was given intravenously (jugular vein), and fluorescence was allowed to reach a steady-state level, as observed in individual microvessels under incident fluorescence microscopy. The radial profile of fluorescence intensity at the EC surface was digitized and fit by a sigmoidal curve using a least-squares method. The location of the inflection point in the radially decreasing dye intensity curve was taken as the outer edge of the glycocalyx. The surface of the EC was taken as the outer edge of the dark refractive band present near the wall in each microvessel under bright-field trans-illumination. The spatial difference between the inflection point and surface of the EC was taken as the thickness of the glycocalyx. All image processing and measurements were done using ImageJ (National Institutes of Health, Bethesda, MD).

*Hemodynamic measurements.* To quantify changes in the resistance to flow in response to shedding of the glycocalyx within individual capillaries, $V_{RBC}$ and arteriovenous ΔP were measured. $V_{RBC}$ was obtained using the two-slit photometric technique (61). The mean velocity of cells plus plasma ($V_{MEAN}$) was assumed to be proportional to the centerline $V_{RBC}$ and given by $V_{MEAN} = V_{RBC}/1.6$ (39). Upstream-to-downstream ΔP in single capillaries was measured by the dual servo-null technique (28). Finely drawn micropipettes (<5-μm tip diameter) were inserted into side branches of feeding arterioles (20- to 30-μm diameter) and draining venules (25- to 40-μm diameter) to obtain ΔP in individual capillaries. The resistance to flow was determined as $R = \Delta P/Q$, where the volumetric flow $Q = V_{MEAN} \times \pi D^2/4$, and $D$ = microvessel luminal diameter.

Separate experiments were performed to measure $H_{CAP}$ during application of fMLP by direct cell counting of RBCs in capillaries. Video recordings of capillary blood flow were made with a gated charge-coupled device camera (Optronics, Goleta, CA) at high shutter speeds (1/4,000-s or 1/10,000-s exposure time) to obtain the number ($N$) of flowing red cells resident at any instant. $H_{CAP}$ was calculated as $H_{CAP} = N \times mcv/(\pi D^2 \times L/4)$, where mcv is mean cell volume, and $D$ and $L$ are capillary diameter and length, respectively. A value of mcv equal to 55 fl was used.

*Statistics.* Statistical analyses of trends in the data were performed using SigmaStat (Systat, San Jose, CA) with either Student's $t$-test for paired measurements, or the Holm-Sidak method for ANOVA of multiple comparisons. Nonparametric tests were used when appropriate, as indicated.

## RESULTS

*Fluorescence intensity measurements.* Measurement of fluorescence intensity of fluorophores in living tissues under laser illumination necessitates correction for the uneven illumination in the microscope field. To illustrate, shown in Fig. 1*A* is a plot of fluorescence intensity in the focal plane ($x$-$y$) of the microscope when focused on the midplane of a 100-μm deep microcuvette containing 0.01 mg/ml fluorescently labeled BS-1 lectin. The nonuniform laser excitation results in a parabolic distribution of emission intensity, $I(x,y)_{uniform}$, for this uniform distribution of fluorophores, with a range of fluorescent intensities from 22 to 994 and a coefficient of variation equal to 17.2%. To correct for this artifact, each image scene was flattened by scaling the input image, $I(x,y)_{in}$, with the algorithm $I(x,y)_{out} = [I(x,y)_{in} - I(x,y)_0]/[I(x,y)_{uniform} - I(x,y)_0] \times K$, where $I(x,y)_0$ is background intensity (no incident illumination), and $K$ is an arbitrary constant, typically taken as 520. Application of this algorithm to the uniform field (Fig. 1*A*) resulted in the flat field of Fig. 1*B*, with an intensity range of 332–649, and a coefficient of variation equal to 1.1%.

The linearity of $I(x,y)_{out}$ with varying fluorophore concentrations was validated by regression of fluorescence intensity against serial dilutions of a known concentration of labeled BS-1. A representative regression of average fluorescence intensity obtained over a 100 $\mu m^2$ area against concentrations of BS-1 ranging from 10 to 175 μg/ml is illustrated in Fig. 1*C*. Intensity was linear with concentration with a regression coefficient of $r^2 = 0.998$ and a root-mean-square error of 6.5%. An illustrative video scene of a capillary image corrected by flattening the field and subtracting off the background intensity (obtained in the avascular tissue space) is shown in Fig. 1*D*. Twenty minutes following infusion of the BS-1, the capillary walls were intensely stained by the fluorophore, which reached steady-state levels. The intensity of the fluorescence was nonuniform because of the shallow depth of field of the objective, estimated to be on the order of 3 μm. The noncircular cross section of microvessels resulted in one wall being in sharp focus at the apex of its curvature, while the other wall obliquely traversed the focal plane, which resulted in a less intense image. Variations in intensity also arose from the entire plane of the vessel being oblique to the focal plane, as illustrated by the microvessel running horizontally in the image

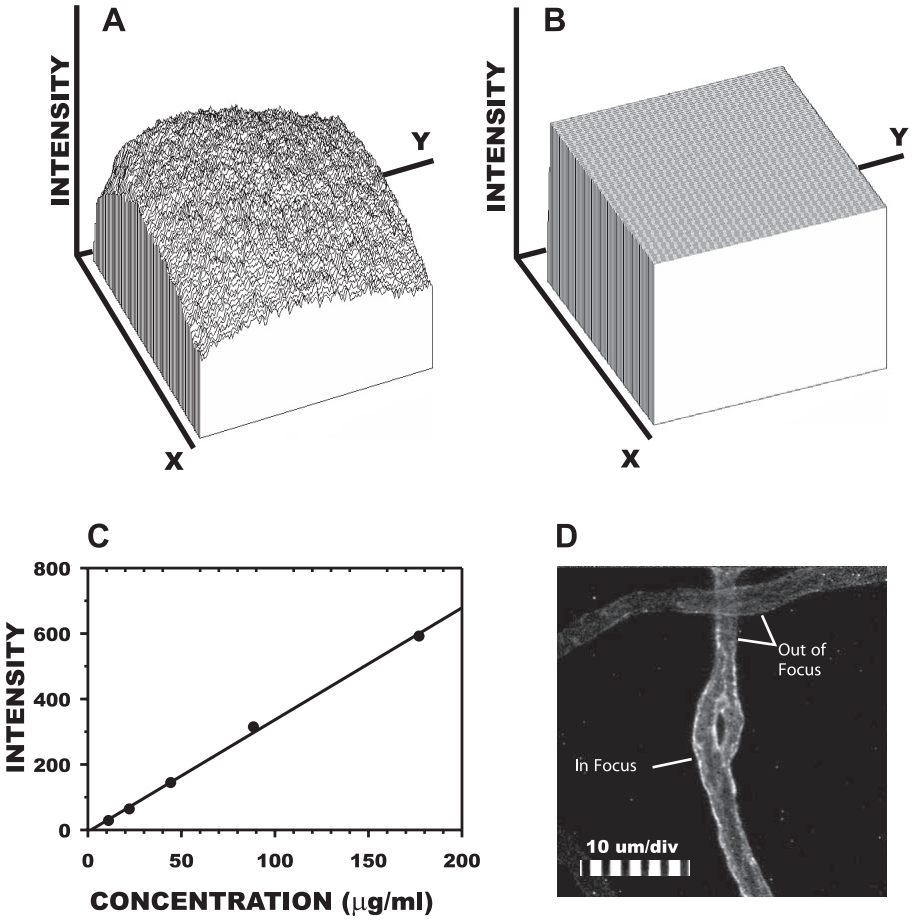


Fig. 1. Schema of image processing for fluorescence intensity measurements. *A*: spatial distribution of fluorescence intensity from a microcuvette containing a 1% solution of the lectin BS-1 conjugated with Alexa Fluor 488. Within the microscope focal plane ($x$–$y$ = 1,024 × 1,024 pixels), emission intensity averaged 691.4 (maximum value = 1,024), with a coefficient of variation of 17.2%. *B*: flattening the field by postprocessing reduced this nonuniformity to 1.1%. *C*: representative calibration of emission intensity vs. BS-1 concentration for corrected images yielded a linear regression with $r^2 = 0.998$ and a root-mean-square error of 6.5%. *D*: representative processed image of a capillary stained with BS-1 (intravenous). The surface of the endothelium within the focal plane stained brightly (*left* wall *above*), whereas portions of the vessel out of focus stained less intensely, as indicated by the *right* wall and the entire capillary at the *top* of the picture.

field at the top. This vessel appeared to be in a focal plane above the vertically running capillary and, as a result, fluoresced much less intensely compared with the capillary. These three-dimensional variations in intensity necessitated multiple sampling at different focal plane positions to obtain an average intensity for a specific microvessel.

*Quantifying lectins bound to the endothelium.* Fluorescence intensity of the bound BS-1 was monitored in arterioles, capillaries, and venules during infusion of the BS-1, during a 20-min period of its binding to the endothelium (EC) and for 30 min following onset of superfusion of the tissue with fMLP. Illustrated in Fig. 2 are representative images of an arteriolar and venular bifurcation during this sequence of events. To reduce the influence of random noise in the intensified image, each image was averaged in real time over 16 successive frames (taken at 30 frames/s) and thus represents the average intensity acquired in a 0.53-s period. Initial studies of the accumulation of BS-1 on the EC revealed that a steady-state level of staining was achieved within 20 min of circulation of the lectin. Hence, all experiments included a 20-min stabilization period before onset of the fMLP. Following superfusion with fMLP, the fluorescence intensity steadily declined, although visual evidence is difficult to discern compared with analysis of the digitized intensity. White blood cells (WBCs) also took up the lectin stain, as shown for WBCs briefly sequestered in the arterioles and their prolonged and firm adhesion in the venules. Also noted is the occurrence of a slight arteriolar vasoconstriction due to the fMLP within the first 5 min and its subsequent lessening over a 30-min period. Prior studies have shown this response to have an insignificant effect on arteriolar resistance (28). Both the time course of vasoconstriction and WBC firm adhesion to the EC were consistent with prior observations of the effects of fMLP (28). Firm adhesion of WBCs in the postcapillary venules reached a maximum within a 15- to 30-min period following onset of superfusion with fMLP.

The accumulation of fluorescently labeled BS-1 on the EC wall was quantified as illustrated in Fig. 3 by a three-step procedure. First, a measurement path was digitally traced by eye along the curvature of the microvessel wall (Fig. 3*A*) and typically ranged from 30 to 100 μm in length. In this example, the measurement path was 240 pixels in length (the equivalent of 40.3 μm), and in other cases ranged from 100 to 900 pixels. A radial line, normal to the measurement path, was then delineated by prescribing a measurement line of sufficient length to span the entire microvessel width and beyond. A custom macro in ImageJ was then executed to sample image intensity in each pixel along the measurement line. The location of the measurement line was then moved to the next pixel along the measurement path, and a second set of radial intensities was digitized. This process was repeated along the entire measurement path (in this case, 240 times), and an average radial intensity distribution was computed. The image formed by the matrix of radial measurement lines is shown in Fig. 3*B*, and the average intensity is given in panel *C*. As shown, the wall delimited by the measurement path became straightened out, and the peak intensity at the wall corresponded to the peak in the radial profile of Fig. 3*C*. In cases in which both walls were in focus in the same image, this process was repeated by drawing a new measurement path line along the opposite wall, and its peak intensity was determined. The peak intensity at the wall was taken as the average of the values for the two walls. If the opposite wall was not in focus, the intensity was either taken as that of the one wall, or another digitized scene was used in which the wall was brought into sharp focus.

Peak wall intensity measurements in 14 arterioles, 50 capillaries, and 17 venules are presented in Fig. 4. Also shown are separate control (sham) experiments, where BS-1 accumula-

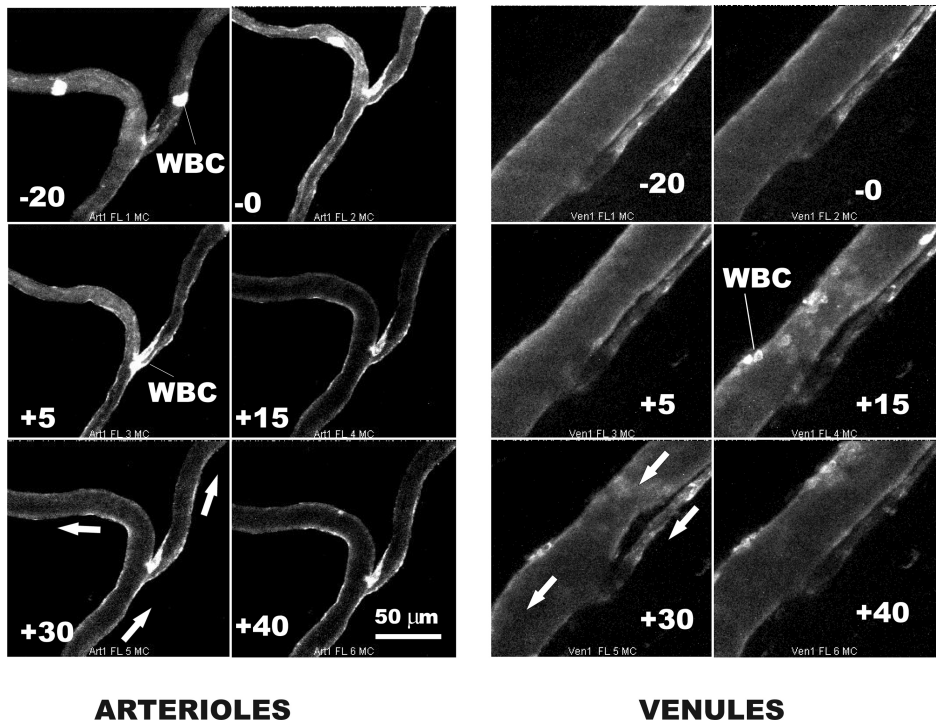


Fig. 2. Representative staining of arterioles and venules in response to a 20-min accumulation of BS-1 conjugated with Alexa Fluor 488. Nominal relative times ($t$) of image acquisition are indicated. At $t = 0$, superfusion of the tissue with $10^{-7}$ M fMLP was begun. The direction of red cell flow is indicated by the arrows. The intermittent adhesion of a white blood cell (WBC) can be seen in arteriole branches, and WBC firm adhesion is strikingly evident in venules following onset of fMLP.

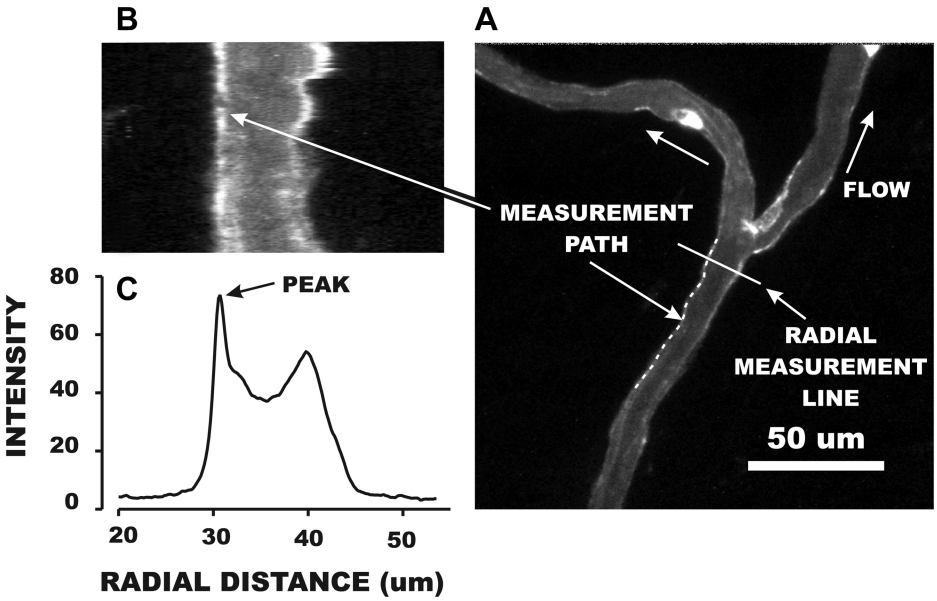


Fig. 3. Illustrative example of quantifying the intensity of BS-1 staining on the microvessel surface. *A*: a measurement path was manually traced along the wall of a vessel (240 pixels in length in this example), and a radial measurement line was automatically generated normal to the beginning of the trace. A computer algorithm averaged the radial intensity distribution at each of the 240 pixels. The rasterized display of each intensity distribution is shown in *B*, and the resultant profile of average intensity is shown in *C*. The effect of the measurement process was to straighten out the wall delimited by the measurement path. The peak intensity was taken as a measure of lectin accumulation and averaged with the peak intensity obtained from an image with the contralateral wall in focus.

tion and fluorescence intensity were monitored during a similar time period without fMLP. The abscissa values for time correspond to the average acquisition time of the images following onset of superfusion of fMLP or controls, which varied by approximately ±5–10 min while scanning multiple tissue regions. Baseline values of intensity before onset of fMLP are given in Table 1. As shown there, capillary baseline intensity was significantly greater than those for either arterioles or venules, $P < 0.02$ (ANOVA). However, a regression analysis of intensity vs. microvessel diameter revealed an insignificant correlation: $r^2 = 0.026$, $P = 0.260$. This behavior suggests that the greater capillary intensity, and hence uptake of lectin, may be due to factors other than optical (e.g., depth of field) or geometric (e.g., departure from a circular lumen) parameters, as noted in the DISCUSSION.

Under control conditions, no statistically significant variation of intensity was observed throughout the 30-min period for each class of microvessel (ANOVA, $P = 0.876$). However, with fMLP superfusion, the intensity in all microvessels fell significantly during the first 5 min and exhibited a significant decline over the 30-min superfusion period, ANOVA, $P < 0.05$. This behavior suggests that the shedding of glycans in response to fMLP was not unique to the venular wall, but common to arterioles, capillaries, and venules.

*Thickness changes of the glycocalyx.* To characterize changes in thickness of the glycocalyx attendant to glycan shedding in response to fMLP, following 20 min superfusion with fMLP fluorescently labeled Dx70 was infused systemically and allowed to equilibrate for 10 min, following which thickness measurements were made, as described in MATERIALS AND METHODS. Thicknesses for 12 arterioles, 24 capillaries, and 12 venules are shown in Fig. 5. Diameters of these microvessels averaged 18.0 ± 3.3 (SD) μm for the arterioles, 8.2 ± 2.0 (SD) μm for the capillaries, and 20.9 ± 8.3 (SD) μm for the venules. Thickness of the glycocalyx before application of fMLP varied significantly among the three orders of microvessels, $P < 0.001$, ANOVA. Statistically, thickness in the capillaries (348 nm) was significantly less than that in arterioles (551 nm) or venules (638 nm), $P < 0.025$, ANOVA. The arterioles were not significantly different from the venules, $P = 0.050$. Paired measurements of thickness before and following fMLP within individual microvessels fell significantly in all three divisions, with ratios of post- to pre-fMLP thickness of 0.74 ± 0.16, 0.88 ± 0.51, and 0.87 ± 0.46 (SD), for arterioles, capillaries, and venules, respectively. The maximum fall occurred in arterioles (26%), followed by venules (13%) and capillaries (12%), with all decreases being statistically significant, $P < 0.05$.

*Hemodynamic measurements and hematocrit.* To assess the impact of alterations in the thickness of the glycocalyx on capillary hemodynamics, two sets of measurements were made: *1*) $V_{RBC}$ and Q values in arterioles, capillaries, and venules; and *2*) ΔP, $V_{RBC}$, and resistance to flow, before and following application of fMLP. Baseline hemodynamic values for the measured ($V_{RBC}$, ΔP, and diameter) and calculated parameters [wall shear rate ($\dot{\gamma}$), Q, and resistance] are given for the two experiments in Table 1. The effect of fMLP on the distribution of flows throughout the hierarchy of arterioles, capillaries, and venules is illustrated in Fig. 6*A*. With application of fMLP, Q fell ~18% in arterioles, which was statistically insignificant, $P = 0.690$. Small yet insignificant decreases in flow also occurred in the capillaries (20%, $P = 0.337$) and venules (3%, $P = 0.941$). To assess the effects of fMLP on the redistribution of flow throughout the mesenteric network, the ratio of capillary ($Q_{CAP}$) and venular flows ($Q_{VEN}$) to their respective feeding arteriolar flows ($Q_{ART}$) is given in Fig. 6*B*. In general, $Q_{CAP}$ and $Q_{VEN}$ changes were proportional to $Q_{ART}$, as evidenced by the constancy of their fractions of $Q_{ART}$. The ratio of $Q_{CAP}$ to $Q_{ART}$ after fMLP to its control value was insignificantly different from 1.0, $P = 0.375$. A similar invariance of $Q_{VEN}$-to-$Q_{ART}$ ratio, $Q_{VEN}/Q_{ART}$, was evident, $P = 0.195$. Hence, it appeared that $Q_{CAP}$ were not disproportionately affected by changes in the glycocalyx of the smaller capillary lumen.

Measurements of $H_{CAP}$ in response to fMLP are given in Table 2 for 31 capillaries studied in three animals with a systemic hematocrit (large vessel) averaging 43 ± 3.6% (SD). Although there was a 22% decrease in $H_{CAP}$ and a 20% decrease in $H_{CAP}$-to-systemic hematocrit ratio following

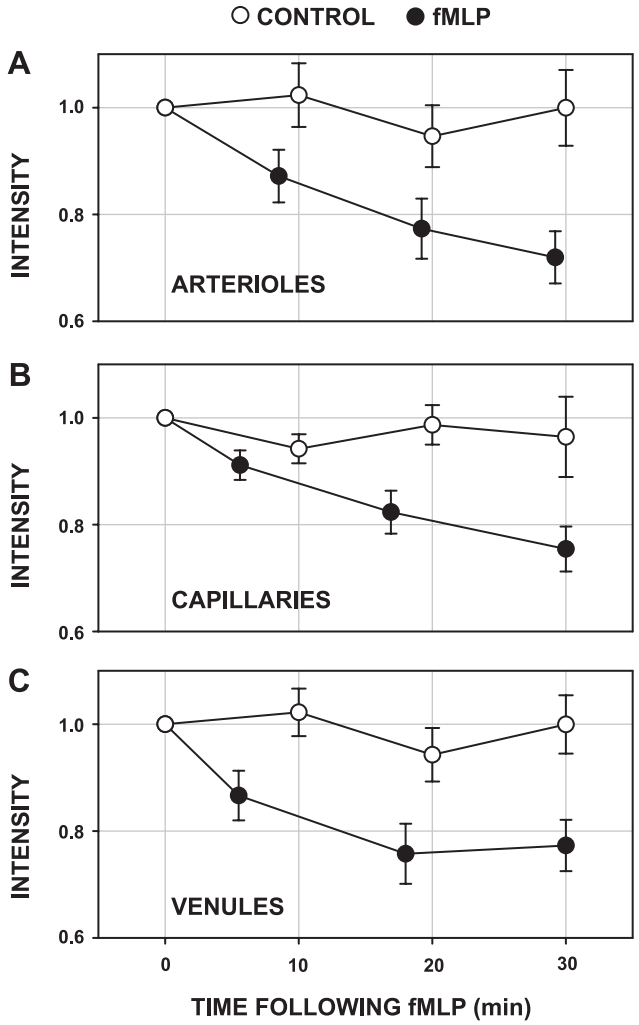


Fig. 4. Shedding of the endothelial glycocalyx in arterioles ($n$ = 14; *A*), capillaries ($n$ = 50; *B*), and venules ($n$ = 17; *C*). The variation of fluorescence intensity with time (●) following onset of superfusion of the mesentery with $10^{-7}$ M fMLP is shown. Peak intensity of fluorescence emission at the endothelial surface was normalized with respect to baseline values before onset of fMLP (Table 1). In each case, intensity fell significantly during the first 5–7 min and during a subsequent 30-min period. Control (sham) experiments conducted over a 30-min period (Ringer solution alone; ○) showed no significant decline in intensity for 21 arterioles, 39 capillaries, and 20 venules. Values are means ± SE.

fMLP, they were not significant, $P = 0.077$ and $P = 0.052$, respectively. For a subset of 21 capillaries, for which paired measurements of $H_{CAP}$ were obtained, the post-to-pre-fMLP ratio was not significantly different from 1.0, $P = 0.801$, Mann-Whitney rank-sum test.

To elucidate the hemodynamic significance of changes in glycocalyx thickness in the capillaries directly, resistance measurements were made in 18 capillaries (Fig. 7). $V_{RBC}$ and $\dot{\gamma}$ fell significantly by ~7%, flow ($Q_{CAP}$) decreased by 5%, and $\Delta P$ rose by 5%, as evidenced by the ratio of their post- to pre-fMLP values. These changes were not significant, as assessed by paired *t*-test. However, an 18% rise in resistance ($R = \Delta P/Q_{CAP}$) was significant, $P < 0.05$. This slight rise in resistance may be due to activation of WBCs by the fMLP, which caused them to stiffen, thus increasing the resistance to flow as they entered the capillaries.

Table 1. *Baseline measurements before superfusion with fMLP*

| | Arterioles | Capillaries | Venules |
|---|---|---|---|
| *Fluorescence intensity measurements (Fig. 4)* | | | |
| No. of vessels | 14 | 50 | 17 |
| Baseline fluorescence intensity | 71.9 ± 47.0 | 133.2 ± 101.1 | 73.9 ± 46.0 |
| Diameter before fMLP, μm | 17.1 ± 6.4 | 8.8 ± 2.5 | 28.8 ± 14.8 |
| No. of control (sham) vessels | 21 | 39 | 20 |
| Diameter of control (sham) vessels, μm | 14.9 ± 6.0 | 9.1 ± 2.5 | 28.2 ± 13.9 |
| *Hemodynamic baseline measurements (Fig. 6)* | | | |
| No. of vessels | 14 | 49 | 16 |
| Diameter, μm | 20.7 ± 9.1 | 9.1 ± 2.7 | 27.0 ± 8.4 |
| $V_{RBC}$, mm/s | 3.3 ± 2.1 | 2.2 ± 1.8 | 1.4 ± 0.9 |
| $\dot{\gamma}$, $s^{-1}$ | 831 ± 525 | 1,266 ± 1111 | 247 ± 162 |
| Q, $10^{-4}$ $mm^3/s$ | 10.8 ± 14.6 | 1.03 ± 1.20 | 6.2 ± 7.0 |
| *ΔP and resistance measurements (Figs. 7 and 8)* | | | |
| No. of vessels | | 18 | |
| Diameter, μm | | 6.7 ± 1.1 | |
| DP, $cmH_2O$ | | 24.1 ± 2.8 | |
| $V_{RBC}$, mm/s | | 1.7 ± 0.7 | |
| $\dot{\gamma}$, $s^{-1}$ | | 1,566 ± 637 | |
| Q, $10^{-4}$ $mm^3/s$ | | 0.6 ± 0.4 | |
| R, $10^5$ $cmH_2O \cdot mm^{-3} \cdot s^{-1}$ | | 5.1 ± 2.5 | |

Values are means ± SD. ΔP, pressure drop; $V_{RBC}$, red cell velocity; $\dot{\gamma}$, shear rate; Q, volume flow; R, resistance.

Presented in Fig. 8 is the ratio of post- to pre-capillary resistance, $R_{POST}/R_{PRE}$, for these 18 capillaries, plotted against capillary diameter (*A*) and the time duration of exposure to fMLP (*B*). Average baseline resistance (pre-fMLP) is given in Table 1. Individual anatomic capillary diameter remained invariant with superfusion of fMLP and averaged 6.69 ± 1.06 (SD) μm before fMLP, and 6.74 ± 1.12 (SD) μm during fMLP, which were not significantly different, $P = 0.663$. With increasing diameter (Fig. 8*A*), $R_{POST}/R_{PRE}$ showed a slight (although insignificant decline, $r^2 = 0.112$, $P = 0.175$), sug-

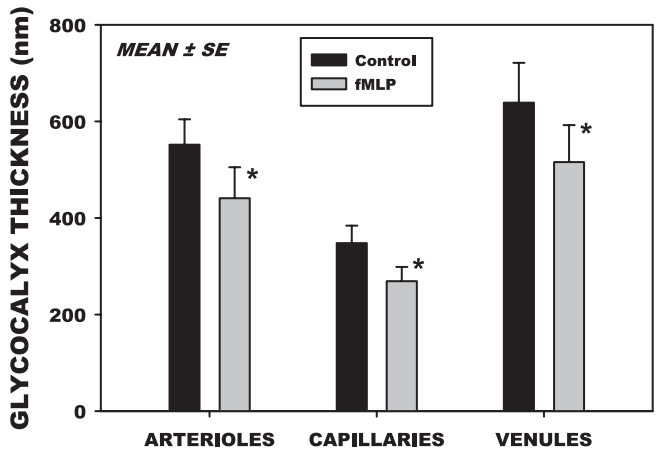


Fig. 5. Changes in the thickness of the glycocalyx measured by the infiltration of FITC labeled dextran 70 kDa into the endothelial surface layer. Thickness was taken as the distance between the edge of the dextran column and the surface of the endothelium for 12 arterioles, 24 capillaries, and 17 venules. Thickness in the capillaries was significantly smaller compared with that of arterioles or venules, $P < 0.025$, ANOVA. In all three divisions of the microvasculature, thickness decreased significantly following superfusion with $10^{-7}$ M fMLP. Values are means ± SE. *$P < 0.05$.

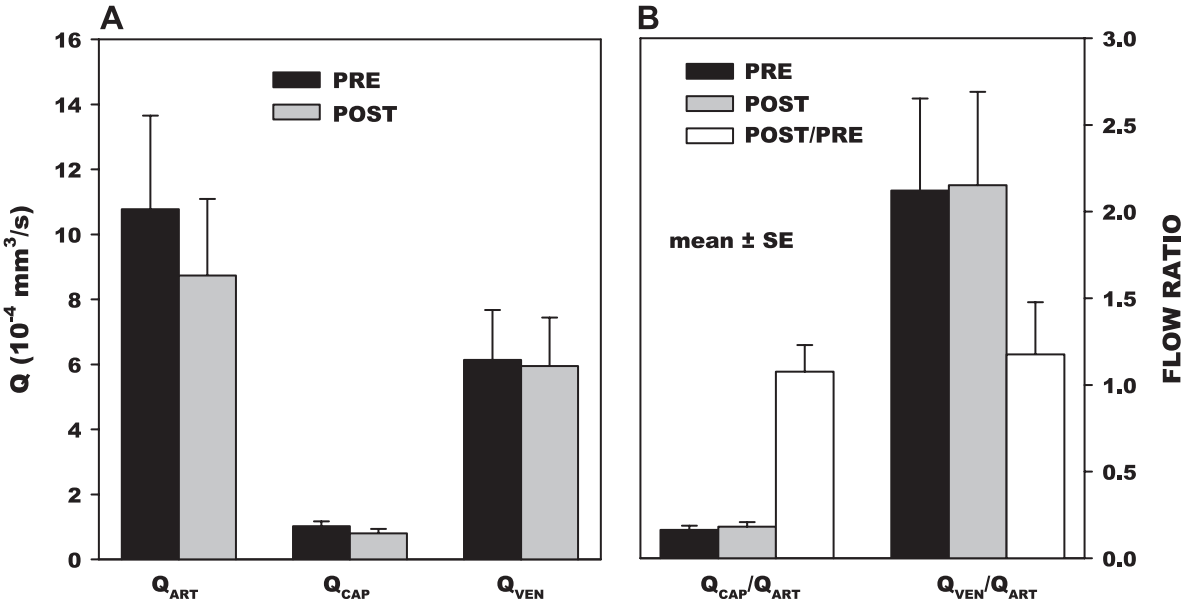


Fig. 6. *A*: calculated volumetric flow rates (Q) measured before and 10–20 min following onset of superfusion of mesentery with $10^{-7}$ M fMLP for 14 arterioles ($Q_{ART}$), 49 capillaries ($Q_{CAP}$), and 16 venules ($Q_{VEN}$). Baseline hemodynamic parameters [red blood cell velocity ($V_{RBC}$), shear rate ($\dot{\gamma}$), and Q] are given in Table 1. A small, yet insignificant, decrease in Q occurred in arterioles ($P = 0.690$), capillaries ($P = 0.337$), and venules ($P = 0.941$). *B*: effects of fMLP on changes in capillary and venular flows relative to their paired feeding arterioles are indicated by the paired ratio of $Q_{CAP}/Q_{ART}$ and $Q_{VEN}/Q_{ART}$. No change occurred in the ratio of these parameters following and before the application of fMLP for $Q_{CAP}/Q_{ART}$ ($P = 0.375$) and $Q_{VEN}/Q_{ART}$ ($P = 0.195$), thus suggesting that significant changes in the resistance to flow did not occur between arterioles, capillaries, and venules. Values are means ± SE.

gesting that the initial increase in resistance arose from sources other than diameter, such as the effect of fMLP on WBC deformability. Although a steeper negative regression slope was evident for the group of capillaries with diameters <8 μm, it too was not statistically significant, $r^2 = 0.210$, $P = 0.086$. Given that shedding of the glycocalyx increased with the time duration of exposure to fMLP (Fig. 4), the ratio of $R_{POST}/R_{PRE}$ was examined as a function of time (Fig. 8*B*). These trends occurred during the time course of sampling the capillary network to make the sequence of hemodynamic measurements (velocity, ΔP, etc.), and revealed a significant 26% decrease in capillary resistance over the 30-min duration of fMLP, $r^2 = 0.257$, $P < 0.032$. The average duration of exposure to fMLP for each capillary during this period was 14.4 ± 7.3 (SD) min.

## DISCUSSION

*fMLP and shedding of the glycocalyx.* In the present studies, the loss of lectins (BS-1) bound to the surface of the endothelium has been shown to rapidly occur in response to topical application of fMLP. In prior studies, it has been demonstrated for glass surfaces to which CS has been covalently linked that the adhesion of BS-1-coated fluorescent microspheres could not be disrupted by shear stresses far in excess of physiological limits (100 dyn/cm$^2$), with or without the presence of $10^{-7}$ M fMLP (38). Hence, it is presumed that the loss of bound lectins shown herein signifies shedding of GAGs or glycosylated proteins from the EC surface. This assumption is also supported by prior studies that have correlated fMLP-induced shedding of antibodies for HS and CS bound to the EC surface

Table 2. *Capillary hematocrit measurements pre- and post-fMLP superfusion*

| Parameter | Pre-fMLP | Post-fMLP |
|---|---|---|
| $H_{CAP}$, % | 28.1 ± 13.6 | 21.9 ± 10.7* |
| $H_{CAP}/H_{SYS}$ | 0.64 ± 0.29 | 0.51 ± 0.26† |
| *N* | 31 | 30 |

Values are means ± SD; *N*, no. of measurements. $H_{CAP}$, capillary hematocrit; $H_{SYS}$, systemic hematocrit; $H_{CAP}/H_{SYS}$, ratio of $H_{CAP}$ to $H_{SYS}$. The 22% fall in $H_{CAP}$ and 20% fall in $H_{CAP}/H_{SYS}$ with fMLP were not significant: *$P = 0.077$, †$P = 0.052$. For 21 paired measurements, the ratio of $(H_{CAP}/H_{SYS})_{Post\text{-}fMLP}/(H_{CAP}/H_{SYS})_{Pre\text{-}fMLP}$ was not significantly different from 1.0 ($P = 0.801$, Mann-Whitney rank sum test), as $H_{CAP}$ fell slightly from 23.8 ± 8.2 to 23.2 ± 12.2% with fMLP.

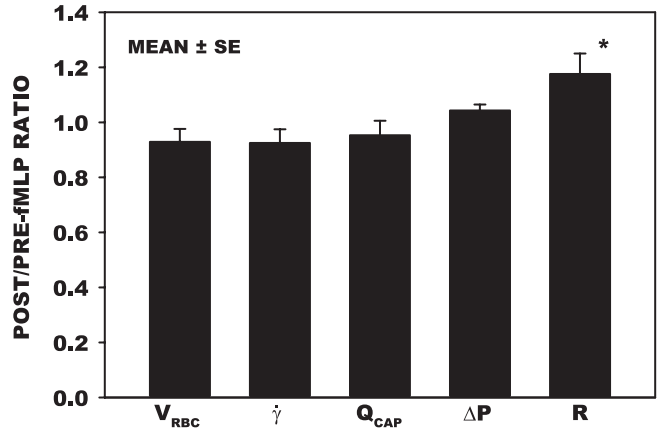


Fig. 7. Post- to pre-fMLP ratios of hemodynamic parameters, $V_{RBC}$, $\dot{\gamma}$, Q, and pressure drop (ΔP) for 18 capillaries measured over a 30-min period of superfusion, with an average duration of 14 min. The corresponding post/pre ratio of the calculated resistance to flow (R = ΔP/Q) is also shown. Post- to pre-fMLP ratios did not change significantly for $V_{RBC}$ ($P = 0.169$), $\dot{\gamma}$ ($P = 0.206$ ), Q ($P = 0.454$), and ΔP ($P = 0.081$), whereas R increased significantly by 18% (*$P < 0.05$), assessed by paired *t*-test. Baseline (pre-fMLP) parameters are given in Table 1. Values are means ± SE.

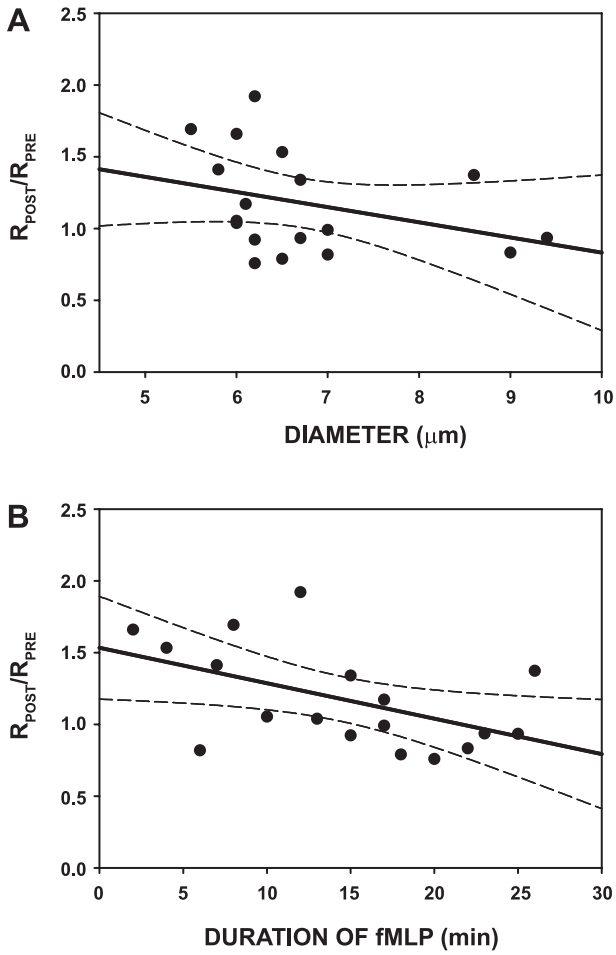


Fig. 8. Post- to pre-fMLP ratio of capillary resistance ($R_{POST}/R_{PRE}$) following onset of superfusion. *A*: values obtained during a 30-min duration of superfusion regressed against capillary luminal diameter (*D*), revealed a regression of $R_{POST}/R_{PRE} = 1.9 - 0.11D$, with $r^2 = 0.112$, which was not significant, $P = 0.175$. (Also shown are 95% confidence intervals, dashed lines.) *B*: regression $R_{POST}/R_{PRE}$ with time duration of superfusion (*t*) revealed a significant regression: $R_{POST}/R_{PRE} = 1.5 - 0.03t$, with $r^2 = 0.257$, $P < 0.032$. The range of times corresponded to the time taken to sample hemodynamic parameters during the experiments. While the average value of $R_{POST}/R_{PRE}$ was elevated 18% (Fig. 7) for the 14-min average duration of fMLP (presumably due to diminished WBC deformability), a significant decrease in resistance ratio over the 30-min period lessened this effect, most likely from shedding of the capillary glycocalyx (Fig. 4), which reduced the resistance to flow.

with shedding of the bound lectins *Bandiera Simplicifolia* (BS-1) and *Lycopersican Esculentum* (43).

The pattern of lectin binding to the EC surface among arterioles, capillaries, and venules may be indicative of the availability of binding sites, as evidenced by the greater intensity of fluorophore at the capillary level (Table 1). However, other factors may influence the delivery and uptake of lectin, which necessitate that agonist-induced changes in intensity be normalized to initial values. Although optical and geometric factors were ruled out (see RESULTS), flow-dependent factors may prevail. For example, wall $\dot{\gamma}$ were typically greatest in the capillaries, compared with the arterioles and venules (Table 1). However, the large spatial variation of capillary $\dot{\gamma}$ throughout the network precluded a statistically significant difference from the arterioles, and the substantially lesser $\dot{\gamma}$ in venules compared with capillaries was significant. Assuming that the deposition and binding of lectin to the EC is convection (flow) limited, the accumulation of lectin over time would be proportional to the volumetric flux per unit of vessel surface area. That is, within a microvessel, the convective flux of lectin with concentration *c* in a stream with Q is given by the product *c*Q, and the area available for its accumulation would be proportional to diameter ($\pi D$). Thus, given that the flux per unit of wall surface area is thus $c\text{Q}/\pi D$ for a tube of unit length, and that for a Newtonian fluid, $\dot{\gamma}$ is given by $32\text{Q}/\pi D^3$, the buildup of lectin may be proportional to $\dot{\gamma}$. While the greater accumulation of lectin in the capillaries is consistent with the higher $\dot{\gamma}$, the equivalence of accumulation between arterioles and venules (Table 1), with markedly different $\dot{\gamma}$ along the wall (Table 1), suggests that other factors may play a role. It is thus conceivable that the increased deposition of lectin on the capillary surface, compared with arterioles and venules, may reflect an increased level of binding sites.

The use of fMLP as an agonist to induce shedding of the glycocalyx stems from its role as a well-studied model of the inflammatory process (3, 28), whereby it mimics a variety of peptides released from either bacterial or host cells during an acute inflammation. It was selected as the agonist for the present studies because of the rapidity of its action and its well documented effect on the mechanical and adhesive properties of WBCs and microvascular hemodynamics. As a stimulus for WBC activation, fMLP causes a stiffening of polymorphonuclear leukocytes (15) and increased polymorphonuclear leukocyte adhesion in postcapillary venules, as a result of stimulation of G protein-coupled receptors (42), and thus significantly increases resistance to flow (28). Based on studies of the rolling and adhesion of WBCs on either artificial surfaces coated with receptors for specific ligands (2, 35, 36), or monolayers of cultured ECs (4, 27, 34), it has long been held that adhesiveness was influenced by regulation of the affinity and avidity of the integrin molecules on the WBC and EC (32, 33, 41, 62). Similar in vivo studies of postcapillary venules in the living animal (3, 28, 37) have supported this concept. The apparent thickness of the glycocalyx has been estimated by the exclusion of erythrocytes and macromolecules (59) to be on the order of 400–500 nm, which significantly exceeds the lengths of EC receptors involved in leukocyte (WBC) rolling on the EC (selectins) and firm adhesion to the EC (integrins). Studies of the lengths of these receptors have shown a range from 20 nm for the $\beta_2$-integrin ligands to 30–40 nm for E- and P-selectins (54). Thus, in view of the concurrent shedding of glycans and increased binding of antibodies to ICAM-1 on the EC in response to fMLP, it has been postulated that stimulated shedding of the glycocalyx may rapidly expose receptors on the EC to facilitate WBC-EC adhesion (43).

The rapid shedding of glycans in response to fMLP in all three divisions of the microvasculature (Fig. 4) suggests that a cascade of signaling events is initiated by EC activation, which is independent of the presence of WBCs. The brief transit time of WBCs in the arteriolar portion of the network (14) and a lack of WBC-EC adhesion in arterioles suggest that the effects of WBC activation are not evident until WBCs reach the true capillaries. Furthermore, it was observed here that shedding of lectins occurred rapidly in venules in which no WBC adhesion occurred, as has been indicated previously by shedding of lectin-coated microspheres (43). Prior studies of the time

course of changes in the composition of the glycocalyx in response to topical application of TNF-α (in hamster cremaster venules) revealed a similar length of time for changes in composition of the glycocalyx, as evidenced by a 30% decrease in thickness of the barrier to infiltration of Dx70 within 20 min, as shown by Henry and Duling (25). In these latter studies, it has also been suggested that TNF-α activates surface bound proteases. This hypothesis is consistent with subsequent observations that fMLP-induced shedding of bound lectins can be inhibited by the matrix metalloproteinase inhibitors, ilomastat and doxycycline (44). The rapidity of shedding of constituents of the glycocalyx in response to TNF-α has also been demonstrated by the rapid outflow of syndecan-1 and HS from the isolated guinea pig coronary circulation (8). Within 5 min of initiation of perfusion with cell-free buffer containing TNF-α, significant amounts of syndecan-1 and HS were found in the effluent, which diminished with time, suggestive of a depletion of components shed from the endothelium.

*Thickness of the glycocalyx.* Using the exclusion of Dx70 as a measure of the thickness of the glycocalyx, changes in response to fMLP were found that are consistent with prior measurements in arterioles, capillaries, and venules of hamster cremaster muscle (24, 25, 59, 60). Although the present measurements appear slightly larger, which may be due to either methodology or species differences, similar trends among vascular divisions between the two species were found. In both preparations, the capillary Dx70 exclusion thickness was smaller than that of either arterioles or venules. The order of magnitude reductions in Dx70 exclusion thickness of 100 nm in arterioles, capillaries, and venules found here (Fig. 5) is consistent with reported venular responses, where the thickness decreased from 400 to 300 nm within 20-min exposure of venules to TNF-α (25). Given that resistance is inversely proportional to the fourth power of diameter, a reduction in capillary diameter from 6.0 to 5.8 μm by the presence of a significant glycocalyx would theoretically increase the resistance to flow by 15%. With larger vessels, for example with a 30-μm diameter, resistance to flow would be increased by only ~3%.

*Network hemodynamics and hematocrit.* To determine whether shedding of the glycocalyx in response to fMLP produced flow redistribution effects due to changes in capillary effective diameter, the relative flow ratios between capillaries and arterioles were examined (Fig. 6). These results suggested that both $Q_{CAP}$ and $Q_{VEN}$ changed in proportion to $Q_{ART}$, and that shedding of the glycocalyx in the smaller diameter capillaries did not measurably affect resistance across the capillary bed. Given the heterogeneity of capillary diameters in mesentery, shunting of flow through larger diameter thoroughfare channels might have lessened the effect of the glycocalyx on the ensemble of capillaries. Overall reductions in flow throughout the microvascular network with fMLP have been shown previously to principally result from obstruction of venules by WBC adhesion and a modest (although insignificant) arteriolar vasoconstriction (28). As shown therein, as few as 12 WBCs adhered to the endothelium per 100 μm of venular length was sufficient to double the resistance to flow. The modest reductions in flow here reflect the substantially lesser amount of WBC-EC adhesion in rat mesentery compared with that in cat (28).

The small, yet insignificant, reductions in $H_{CAP}$ were consistent with prior observations of the effects of fMLP on arterioles and venules (28). As shown therein, no significant change in arteriolar or venular hematocrit occurred with fMLP, as assessed by direct spectrophotometric methods. In contrast, $H_{CAP}$ was found to increase in response to degradation of the glycocalyx twofold with direct infusion of heparinase with micropipettes (13) and systemic infusion of hyaluronidase (7). Systemic infusion of oxidized LDL increased it twofold (10), and sustained epifluorescence illumination increased it by 68% (59), presumably due to generation of reactive oxygen species in both studies. Thus the mechanisms of glycan shedding in these studies might differ from those invoked by fMLP.

*Capillary resistance to flow.* To more precisely delineate changes in flow resistance at the capillary level in response to fMLP, ΔP and flow measurements were made in capillaries. The invariance of capillary hemodynamic parameters ($V_{RBC}$, volume flow, $\dot{\gamma}$, and ΔP) and resistance (Fig. 7) are consistent with the relative changes in flows throughout arteriolar, capillary, and venular divisions of the network. The 18% increase in capillary resistance with fMLP is contrary to the 14–20% decreases in resistance found during enzymatic removal of the glycocalyx by perfusion of the microvascular network with heparinase by Pries et al. (50). This disparity could be due to several factors. Although the two studies examined similar tissues (mesentery of the rat), the ΔP and flows measured across the microvascular networks were strikingly different. In the present study, $Q_{ART}$ on the order of 65 nl/min (1 nl/s in Table 1) were measured in 21-μm-diameter arterioles, compared with 740 nl/min in the experiments by Pries et al. for slightly larger vessels averaging 29 μm. ΔP measured herein were only 17.8 mmHg (24.1 $cmH_2O$, Table 1) compared with 52 mmHg by Pries et al. Thus the baseline resistance to flow measured by Pries et al. was on the order of $0.06 \times 10^5$ $cmH_2O \cdot mm^{-3} \cdot s^{-1}$ (calculated from Table 1 in Pries et al.), which was 1/100th that measured here ($5.1 \times 10^5$ $cmH_2O \cdot mm^{-3} \cdot s^{-1}$, Table 1). This lower resistance is suggestive of a greater number of parallel pathways to carry off the stream. Comparison of the flows between the two studies suggests that there might be 10 times as many pathways between arteriole and venule in the Pries study compared with herein (i.e., 740 compared with 65 nl/min in arterioles). Prior studies by Pries et al. (49) have indeed shown a greater degree of vascularity peculiar to the Wistar rats used in their studies, compared with the strain of Wistar used presently and in previous studies from this laboratory. Hence, from a hemodynamic perspective, the current baseline conditions are reasonably consistent with those of Pries et al. (50). Another source of disparity between the two studies could also be the method for removal of the glycocalyx.

Using direct micropipette infusion of a mixture of heparinase, chondroitinase, and hyaluronidase in postcapillary venules (19), it has been shown that the Dx70 exclusion thickness could be maximally reduced in 40-μm-diameter venules from 463 to 52 nm (~90%). In those studies, superfusion with $10^{-7}$ M fMLP caused a reduction of Dx70 exclusion zone by 130 nm, which is similar in magnitude to the reductions of 110, 80, and 123 nm observed here in arterioles, capillaries, and venules, respectively (Fig. 5). For heparinase alone, the reductions in Dx70 thickness were smaller than the mixture, from 463 to 233 nm, or ~50% (19). Thus it appears unlikely that the resistance

reductions measured by Pries et al. (50) in response to heparinase were entirely from removal of the glycocalyx.

Previous studies on the effects of superfusion of the mesentery with fMLP showed a twofold increase in resistance due to obstruction of the venular lumen with firmly adhered WBCs. In the present studies, no firm adhesion of WBCs was observed in the arterioles or capillaries, although a few transient sequestration events were observed. It is conceivable that these events arose from stiffening of the WBCs as they become activated by the fMLP, and hence their entry time into the capillaries was prolonged, which served to raise capillary resistance. The small, albeit insignificant, decrease in the resistance ratio of post- to pre-fMLP superfusion for the true capillaries with increasing diameter (Fig. 8*A*) supports the hypothesis that diminished WBC deformability is largely responsible for the increase in capillary resistance with fMLP. Less deformable WBCs will take longer to enter a smaller capillary and require a greater $\Delta P$. This effect is well known to depend on the ratio of cell to capillary diameter (15). The smaller the pore size, the greater will be the $\Delta P$ required for the WBC to deform and enter a capillary. Hence, the increase in resistance with WBC stiffening will diminish as diameters become larger. Increased capillary plugging and resistance to flow in the spinotrapezius muscle has been shown in response to superfusion with fMLP, where a 20% increase in capillary resistance was attributed to fMLP activation (22, 23), which is similar to that found here.

A significant decrease in post- to pre-fMLP capillary resistance ($R_{POST}/R_{PRE}$) was found with increased duration of exposure to fMLP (Fig. 8*B*). Based on linear regression of the data, this decrease amounted to 26% over the 30-min duration of superfusion with fMLP. Hence, the overall effect of superfusing the mesentery with fMLP was to raise capillary resistance by diminishing WBC deformability, which was mitigated in time by shedding of the glycocalyx to increase the effective capillary diameter. This level of resistance reduction is thus consistent with that obtained by Pries et al. (50) by stripping off portions of the glycocalyx with heparinase. In contrast, however, the experiments of Chappell et al. (8) revealed an increased resistance to flow concurrent with HS and syndecan-1 shedding in response to TNF-$\alpha$. These latter experiments were done with cell-free solutions, and hence there were no contributions to resistance by WBCs. It is likely that the increase in resistance therein resulted from the observed increase in transvascular fluid exchange attendant to TNF-$\alpha$ which caused edema and compression of capillaries to increase resistance. In the case of fMLP in the absence of WBCs, studies have revealed that no increase in transvascular fluid flux occurs, as assessed by direct measurement of capillary permeability (63).

In summary, the present studies reveal that shedding of the endothelial glycocalyx rapidly occurs within all divisions of the rat mesentery network in response to the chemoattractant fMLP. A concurrent 18% increase in the resistance to flow at the capillary level occurs due to diminished WBC deformability and the added $\Delta P$ required for WBCs to traverse the capillary network. Shedding of the capillary glycocalyx attendant to endothelial activation by fMLP results in an increase in capillary effective diameter and a reduction in capillary resistance that mitigates the effects of WBC stiffening. Thus these events contribute to the overall hemodynamic response during the inflammatory process and suggest that concurrent shedding of the endothelial glycocalyx and diminished WBC deformability are equally important rheological factors that affect $Q_{CAP}$.

## GRANTS

This work was supported by National Heart, Lung, and Blood Institute Research Grant R01 HL-39286-20.

## DISCLOSURES

No conflicts of interest, financial or otherwise, are declared by the author(s).

## AUTHOR CONTRIBUTIONS

Author contributions: H. H. L. conception and design of research; H. H. L., L. G., and A. L. performed experiments; H. H. L., L. G., and A. L. analyzed data; H. H. L. interpreted results of experiments; H. H. L. prepared figures; H. H. L. drafted manuscript; H. H. L. edited and revised manuscript; H. H. L. approved final version of manuscript.

## REFERENCES

1. **Adamson RH.** Permeability of frog mesenteric capillaries after partial pronase digestion of the endothelial glycocalyx. *J Physiol* 428: 1–13, 1990.
2. **Alon R, Hammer DA, Springer TA.** Lifetime of the P-selectin-carbohydrate bond and its response to tensile force in hydrodynamic flow. *Nature* 374: 539–542, 1995.
3. **Arfors KE, Lundberg C, Lindbom L, Lundberg K, Beatty PG, Harlan JM.** A monoclonal antibody to the membrane glycoprotein complex CD18 inhibits polymorphonuclear leukocyte accumulation and plasma leakage in vivo. *Blood* 69: 338–340, 1987.
4. **Arisaka T, Mitsumata M, Kawasumi M, Tohjima T, Hirose S, Yoshida Y.** Effects of shear stress on glycosaminoglycan synthesis in vascular endothelial cells. *Ann N Y Acad Sci* 748: 543–554, 1995.
5. **Becker BF, Chappell D, Bruegger D, Annecke T, Jacob M.** Therapeutic strategies targeting the endothelial glycocalyx: acute deficits, but great potential. *Cardiovasc Res* 87: 300–310, 2010.
6. **Bruegger D, Jacob M, Rehm M, Loetsch M, Welsch U, Conzen P, Becker BF.** Atrial natriuretic peptide induces shedding of endothelial glycocalyx in coronary vascular bed of guinea pig hearts. *Am J Physiol Heart Circ Physiol* 289: H1993–H1999, 2005.
7. **Cabrales P, Vazquez BY, Tsai AG, Intaglietta M.** Microvascular and capillary perfusion following glycocalyx degradation. *J Appl Physiol* 102: 2251–2259, 2007.
8. **Chappell D, Hofmann-Kiefer K, Jacob M, Rehm M, Briegel J, Welsch U, Conzen P, Becker BF.** TNF-alpha induced shedding of the endothelial glycocalyx is prevented by hydrocortisone and antithrombin. *Basic Res Cardiol* 104: 78–89, 2009.
9. **Colburn P, Kobayashi E, Buonassisi V.** Depleted level of heparan sulfate proteoglycan in the extracellular matrix of endothelial cell cultures exposed to endotoxin. *J Cell Physiol* 159: 121–130, 1994.
10. **Constantinescu AA, Vink H, Spaan JA.** Elevated capillary tube hematocrit reflects degradation of endothelial cell glycocalyx by oxidized LDL. *Am J Physiol Heart Circ Physiol* 280: H1051–H1057, 2001.
11. **Constantinescu AA, Vink H, Spaan JA.** Endothelial cell glycocalyx modulates immobilization of leukocytes at the endothelial surface. *Arterioscler Thromb Vasc Biol* 23: 1541–1547, 2003.
12. **Danielli JF.** Capillary permeability and oedema in the perfused frog. *J Physiol* 98: 109–129, 1940.
13. **Desjardins C, Duling BR.** Heparinase treatment suggests a role for the endothelial cell glycocalyx in regulation of capillary hematocrit. *Am J Physiol Heart Circ Physiol* 258: H647–H654, 1990.
14. **Eppihimer MJ, Lipowsky HH.** Leukocyte sequestration in the microvasculature in normal and low flow states. *Am J Physiol Heart Circ Physiol* 267: H1122–H1134, 1994.
15. **Eppihimer MJ, Lipowsky HH.** Effects of leukocyte-capillary plugging on the resistance to flow in the microvasculature of cremaster muscle for normal and activated leukocytes. *Microvasc Res* 51: 187–201, 1996.
16. **Fitzgerald ML, Wang Z, Park PW, Murphy G, Bernfield M.** Shedding of syndecan-1 and -4 ectodomains is regulated by multiple signaling pathways and mediated by a TIMP-3-sensitive metalloproteinase. *J Cell Biol* 148: 811–824, 2000.

17. **Florian JA, Kosky JR, Ainslie K, Pang Z, Dull RO, Tarbell JM.** Heparan sulfate proteoglycan is a mechanosensor on endothelial cells. *Circ Res* 93: e136–e142, 2003.
18. **Fux L, Ilan N, Sanderson RD, Vlodavsky I.** Heparanase: busy at the cell surface. *Trends Biochem Sci* 34: 511–519, 2009.
19. **Gao L, Lipowsky HH.** Composition of the endothelial glycocalyx and its relation to its thickness and diffusion of small solutes. *Microvasc Res* 80: 394–401, 2010.
20. **Gouverneur M, Spaan JA, Pannekoek H, Fontijn RD, Vink H.** Fluid shear stress stimulates incorporation of hyaluronan into endothelial cell glycocalyx. *Am J Physiol Heart Circ Physiol* 290: H458–H462, 2006.
21. **Haldenby KA, Chappell DC, Winlove CP, Parker KH, Firth JA.** Focal and regional variations in the composition of the glycocalyx of large vessel endothelium. *J Vasc Res* 31: 2–9, 1994.
22. **Harris AG, Skalak TC.** Effects of leukocyte activation on capillary hemodynamics in skeletal muscle. *Am J Physiol Heart Circ Physiol* 264: H909–H916, 1993.
23. **Harris AG, Skalak TC, Hatchell DL.** Leukocyte-capillary plugging and network resistance are increased in skeletal muscle of rats with streptozotocin-induced hyperglycemia. *Int J Microcirc Clin Exp* 14: 159–166, 1994.
24. **Henry CB, Duling BR.** Permeation of the luminal capillary glycocalyx is determined by hyaluronan. *Am J Physiol Heart Circ Physiol* 277: H508–H514, 1999.
25. **Henry CB, Duling BR.** TNF-alpha increases entry of macromolecules into luminal endothelial cell glycocalyx. *Am J Physiol Heart Circ Physiol* 279: H2815–H2823, 2000.
26. **Hofmann-Kiefer KF, Kemming GI, Chappell D, Flondor M, Kisch-Wedel H, Hauser A, Pallivathukal S, Conzen P, Rehm M.** Serum heparan sulfate levels are elevated in endotoxemia. *Eur J Med Res* 14: 526–531, 2009.
27. **Hoover RL, Folger R, Haering WA, Ware BR, Karnovsky MJ.** Adhesion of leukocytes to endothelium: roles of divalent cations, surface charge, chemotactic agents and substrate. *J Cell Sci* 45: 73–86, 1980.
28. **House SD, Lipowsky HH.** Leukocyte-endothelium adhesion: microhemodynamics in mesentery of the cat. *Microvasc Res* 34: 363–379, 1987.
29. **Huxley VH, Williams DA.** Role of a glycocalyx on coronary arteriole permeability to proteins: evidence from enzyme treatments. *Am J Physiol Heart Circ Physiol* 278: H1177–H1185, 2000.
30. **Ihrcke NS, Platt JL.** Shedding of heparan sulfate proteoglycan by stimulated endothelial cells: evidence for proteolysis of cell-surface molecules. *J Cell Physiol* 168: 625–637, 1996.
31. **Ihrcke NS, Wrenshall LE, Lindman BJ, Platt JL.** Role of heparan sulfate in immune system-blood vessel interactions. *Immunol Today* 14: 500–505, 1993.
32. **Kinashi T, Katagiri K.** Regulation of lymphocyte adhesion and migration by the small GTPase Rap1 and its effector molecule, RAPL. *Immunol Lett* 93: 1–5, 2004.
33. **Laudanna C, Kim JY, Constantin G, Butcher E.** Rapid leukocyte integrin activation by chemokines. *Immunol Rev* 186: 37–46, 2002.
34. **Lawrence MB, McIntire LV, Eskin SG.** Effect of flow on polymorphonuclear leukocyte/endothelial cell adhesion. *Blood* 70: 1284–1290, 1987.
35. **Lawrence MB, Springer TA.** Leukocytes roll on a selectin at physiologic flow rates: distinction from and prerequisite for adhesion through integrins. *Cell* 65: 859–873, 1991.
36. **Lawrence MB, Springer TA.** Neutrophils roll on E-selectin. *J Immunol* 151: 6338–6346, 1993.
37. **Ley K, Bullard DC, Arbones ML, Bosse R, Vestweber D, Tedder TF, Beaudet AL.** Sequential contribution of L- and P-selectin to leukocyte rolling in vivo. *J Exp Med* 181: 669–675, 1995.
38. **Lipowsky HH, Haynes CA.** Synthesis of an artificial glycocalyx for studies of leukocyte adhesion (Abstract). In: *Proceedings of the 2005 Summer Bioengineering Conference, Vail, CO, June 22–26*. New York: American Society of Mechanical Engineers, 2005, p. 247851.
39. **Lipowsky HH, Zweifach BW.** Application of the "two-slit" photometric technique to the measurement of microvascular volumetric flow rates. *Microvasc Res* 15: 93–101, 1978.
40. **Luft JH.** Fine structures of capillary and endocapillary layer as revealed by ruthenium red. *Fed Proc* 25: 1773–1783, 1966.
41. **Luo BH, Carman CV, Springer TA.** Structural basis of integrin regulation and signaling. *Annu Rev Immunol* 25: 619–647, 2007.
42. **Mulivor AW, Lipowsky HH.** Role of glycocalyx in leukocyte-endothelial cell adhesion. *Am J Physiol Heart Circ Physiol* 283: H1282–H1291, 2002.
43. **Mulivor AW, Lipowsky HH.** Inflammation- and ischemia-induced shedding of venular glycocalyx. *Am J Physiol Heart Circ Physiol* 286: H1672–H1680, 2004.
44. **Mulivor AW, Lipowsky HH.** Inhibition of glycan shedding and leukocyte-endothelial adhesion in postcapillary venules by suppression of matrixmetalloprotease activity with doxycycline. *Microcirculation* 1–10, 2009.
45. **Park PW, Reizes O, Bernfield M.** Cell surface heparan sulfate proteoglycans: selective regulators of ligand-receptor encounters. *J Biol Chem* 275: 29923–29926, 2000.
46. **Platt JL, Dalmasso AP, Lindman BJ, Ihrcke NS, Bach FH.** The role of C5a and antibody in the release of heparan sulfate from endothelial cells. *Eur J Immunol* 21: 2887–2890, 1991.
47. **Platt JL, Vercellotti GM, Lindman BJ, Oegema TR Jr, Bach FH, Dalmasso AP.** Release of heparan sulfate from endothelial cells. Implications for pathogenesis of hyperacute rejection. *J Exp Med* 171: 1363–1368, 1990.
48. **Pries AR, Secomb TW, Gaehtgens P.** The endothelial surface layer. *Pflügers Arch* 440: 653–666, 2000.
49. **Pries AR, Secomb TW, Gessner T, Sperandio MB, Gross JF, Gaehtgens P.** Resistance to blood flow in microvessels in vivo. *Circ Res* 75: 904–915, 1994.
50. **Pries AR, Secomb TW, Jacobs H, Sperandio M, Osterloh K, Gaehtgens P.** Microvascular blood flow resistance: role of endothelial surface layer. *Am J Physiol Heart Circ Physiol* 273: H2272–H2279, 1997.
51. **Rehm M, Bruegger D, Christ F, Conzen P, Thiel M, Jacob M, Chappell D, Stoeckelhuber M, Welsch U, Reichart B, Peter K, Becker BF.** Shedding of the endothelial glycocalyx in patients undergoing major vascular surgery with global and regional ischemia. *Circulation* 116: 1896–1906, 2007.
52. **Reitsma S, Slaaf DW, Vink H, van Zandvoort MA, oude Egbrink MG.** The endothelial glycocalyx: composition, functions, and visualization. *Pflügers Arch* 454: 345–359, 2007.
53. **Saunders S, Jalkanen M, O'Farrell S, Bernfield M.** Molecular cloning of syndecan, an integral membrane proteoglycan. *J Cell Biol* 108: 1547–1556, 1989.
54. **Springer TA.** Adhesion receptors of the immune system. *Nature* 346: 425–434, 1990.
55. **Squire JM, Chew M, Nneji G, Neal C, Barry J, Michel C.** Quasi-periodic substructure in the microvessel endothelial glycocalyx: a possible explanation for molecular filtering? *J Struct Biol* 136: 239–255, 2001.
56. **Subramanian SV, Fitzgerald ML, Bernfield M.** Regulated shedding of syndecan-1 and -4 ectodomains by thrombin and growth factor receptor activation. *J Biol Chem* 272: 14713–14720, 1997.
57. **Svennevig K, Hoel T, Thiara A, Kolset S, Castelheim A, Mollnes T, Brosstad F, Fosse E, Svennevig J.** Syndecan-1 plasma levels during coronary artery bypass surgery with and without cardiopulmonary bypass. *Perfusion* 23: 165–171, 2008.
58. **van Haaren PM, VanBavel E, Vink H, Spaan JA.** Localization of the permeability barrier to solutes in isolated arteries by confocal microscopy. *Am J Physiol Heart Circ Physiol* 285: H2848–H2856, 2003.
59. **Vink H, Duling BR.** Identification of distinct luminal domains for macromolecules, erythrocytes, and leukocytes within mammalian capillaries. *Circ Res* 79: 581–589, 1996.
60. **Vink H, Duling BR.** Capillary endothelial surface layer selectively reduces plasma solute distribution volume. *Am J Physiol Heart Circ Physiol* 278: H285–H289, 2000.
61. **Wayland H, Johnson PC.** Erythrocyte velocity measurement in microvessels by a two-slit photometric method. *J Appl Physiol* 22: 333–337, 1967.
62. **Zarbock A, Ley K.** Neutrophil adhesion and activation under flow. *Microcirculation* 16: 31–42, 2009.
63. **Zhu L, Castranova V, He P.** fMLP-stimulated neutrophils increase endothelial $[Ca^{2+}]_i$ and microvessel permeability in the absence of adhesion: role of reactive oxygen species. *Am J Physiol Heart Circ Physiol* 288: H1331–H1338, 2005.
64. **Zuurbier CJ, Demirci C, Koeman A, Vink H, Ince C.** Short-term hyperglycemia increases endothelial glycocalyx permeability and acutely decreases lineal density of capillaries with flowing red blood cells. *J Appl Physiol* 99: 1471–1476, 2005.